nature

Supplementary information

Initial Upper Palaeolithic *Homo sapiens* from Bacho Kiro Cave, Bulgaria

In the format provided by the authors and unedited

Jean-Jacques Hublin✉, Nikolay Sirakov, Vera Aldeias, Shara Bailey, Edouard Bard, Vincent Delvigne, Elena Endarova, Yoann Fagault, Helen Fewlass, Mateja Hajdinjak, Bernd Kromer, Ivaylo Krumov, João Marreiros, Naomi L. Martisius, Lindsey Paskulin, Virginie Sinet-Mathiot, Matthias Meyer, Svante Pääbo, Vasil Popov, Zeljko Rezek, Svoboda Sirakova, Matthew M. Skinner, Geoff M. Smith, Rosen Spasov, Sahra Talamo, Thibaut Tuna, Lukas Wacker, Frido Welker, Arndt Wilcke, Nikolay Zahariev, Shannon P. McPherron & Tsenka Tsanova

Supplementary Information

Initial Upper Palaeolithic *Homo sapiens* from Bacho Kiro Cave (Bulgaria)

Jean-Jacques Hublin[1,2]*, Nikolay Sirakov[3] ,Vera Aldeias[4], Shara Bailey[1,5], Edouard Bard[6], Vincent Delvigne[7,8], Elena Endarova[9], Yoann Fagault[6], Helen Fewlass[1], Mateja Hajdinjak[9], Bernd Kromer[1], Ivaylo Krumov[10], João Marreiros[4,11], Naomi L. Martisius[12], Lindsey Paskulin[13], Virginie Sinet-Mathiot[1], Matthias Meyer[9], Svante Pääbo[9], Vasil Popov[14], Zeljko Rezek[1,15],Svoboda Sirakova[3], Matthew M. Skinner[1,16], Geoff M. Smith[1], Rosen Spasov[17], Sahra Talamo[1,18], Thibaut Tuna[6], Lukas Wacker[19], Frido Welker[1,20], Arndt Wilcke[21], Nikolay Zahariev[22], Shannon P. McPherron[1], Tsenka Tsanova[1]

1 - Department of Human Evolution, Max Planck Institute for Evolutionary Anthropology, Leipzig, Germany. 2 - Chaire Internationale de Paléoanthropologie, Collège de France, Paris, France.
3 - National Institute of Archaeology with Museum, Bulgarian Academy of Sciences, Sofia, Bulgaria.
4 - Interdisciplinary Centre for Archaeology and the Evolution of Human Behaviour, Universidade do Algarve, Faro, Portugal.
5 - Department of Anthropology, New York University, New York, USA.
6 - CEREGE, Université d'Aix Marseille, CNRS, IRD, INRA, Collège de France,13545 Aix-en-Provence, France
7 - Service de Préhistoire, University of Liège, 4000 Liège, Belgium
8 -University of Bordeaux, CNRS, UMR 5199 PACEA, 33615 Pessac, France
9 - Department of Evolutionary Genetics, Max Planck Institute for Evolutionary Anthropology, Leipzig, Germany.
10 - History Museum Belogradchik, Bulgaria.
11 - TraCEr, Monrepos Archaeological Research Centre and Museum for Human Behavioural Evolution, RGZM, Mainz, Germany.
12 - Department of Anthropology, University of California, Davis, USA.
13 - Department of Archaeology, University of Aberdeen, United Kingdom.
14 - Institute of Biodiversity and Ecosystem Research, Bulgarian Academy of Sciences, Sofia, Bulgaria.
15 - University of Pennsylvania Museum of Archaeology and Anthropology, Philadelphia, PA, USA.
16 - School of Anthropology and Conservation, University of Kent, United Kingdom.
17 - Archaeology Department, New Bulgarian University, Sofia, Bulgaria.
18 - Department of Chemistry "G. Ciamician", University of Bologna, Via Selmi, 2, I-40126 Bologna, Italy.
29 - Department of Earth Sciences, ETH Zurich, Switzerland.
20 - Section for Evolutionary Genomics, Globe Institute, University of Copenhagen, Denmark.
21 - Department of Cell Therapy, Fraunhofer Institute for Cell Therapy and Immunology, Leipzig, Germany.
22 - New Bulgarian University, Archaeology Department, Sofia, Bulgaria.

*Correspondence to: hublin@eva.mpg.de

Supplementary Information

Contents

Supplementary Discussion 1: Stratigraphy and Site Formation

SI Fig. 1 shows the profiles exposed during our excavations at Bacho Kiro Cave. This area is the entrance of a large karstic system that extends for more than 3 km. The bedrock slopes from the interior to the cave's entrance, roughly from south to north. The sequence is divided into several layers, which are, in turn, grouped into three main Lithostratigraphic Units (henceforth, LU). Within each major LU are layer subdivisions: K, J and I (Lower LU), H and G (Middle LU) and F, E, D, C, B, A (Upper LU). Layers of the Lower LU fill in topographic depressions in the cave's floor and rest against the bedrock as it rises towards the south. Therefore, in the Main Sector, Layer J was identified along grid lines E/F 5/6, though by grid line G 5/4 Layer G rests directly on bedrock. In the Niche 1, where the bedrock floor is lower than in the Main Sector, Layers K, J and I are better represented, with Layer K resting on bedrock. In-depth site formation analysis of the sequence is ongoing. Here we present preliminary observations on the sedimentary and post-depositional processes of the Lower LU – Layers K, J, I – and its contact with the Middle LU – Layers H and G. While the two excavation areas are no longer physically connected, there is stratigraphic correspondence between the Middle and Lower LUs in Niche 1 and the Main Sector (SI Tab. 1), and these will be described together here.

Lower LU: Layer K

Layer K comprises loamy sands with a relatively low density of Middle Palaeolithic artefacts and common limestone clasts. Under the microscope, these deposits are composed of abundant phosphatic coprolite grains dispersed throughout the deposits, rare bones and limestone fragments. Partial decalcification of limestone clasts (loss of carbonates) is commonly observed (SI Fig. 2). Rare yellowish isotropic domains and stringers were identified in the groundmass. There is a common orientation of the clay particles around coarser components (granostriated b-fabric). These characteristics point to shear deformation associated with wetting and drying conditions, favouring partial dissolution of carbonate content. Sedimentary sources relate to local spalling of the limestone roof and walls, with sands and silts being reworked through slope processes from inside the karstic system. The contact with Layer J above is gradual (SI Fig. 3).

Lower LU: Layer J

Layer J is greenish brown loamy clay with continued local contribution of roof fall clasts up to 20 cm wide. As in Layer K, the deposits are also subject to decalcification and contain coprolite grains – though locally less frequent than in Layer K. Towards its top, Layer J tends to be richer in limestone clasts and granules. In some areas, large cm-sized bones and few charcoals are observed. Calcified root casts (rhizoliths) were identified in thin section. Although there is no major change in sedimentation, preliminary micromorphological analyses show the presence of

thin and crudely bedded lenses (SI Fig. 3 and 4) and local domains with 1-2 cm thick laminae of isotropic material consisting of manganese coatings (SI Fig. 3). These features point to low-energy sheet wash occasionally affecting exposed surfaces and possible ponding, which suggests that there were temporal hiatuses and sporadic accumulation through the sedimentary accretion of Layer J. The main sedimentary sources continue to be from inside the karst system towards this cave entrance area. The contact between Layers J and I is sharp and clear, particularly in the Niche 1 Sector. In the Main Sector, both Layers J and I are thinner, abutting against the rising bedrock floor and locally associated with dm-sized roof fall (SI Fig. 5). SI Fig. 4 shows the contact between Layers J and I in thin section.

Lower LU: Layer I

From both macro (in the field) and micro (micromorphology) perspectives, Layer I is a diagnostic dark brown loamy clay, which is extremely rich in archaeological remains (SI Fig. 5). The deposits are composed of a jumble of anthropogenically deposited material, namely abundant bone fragments (some thermally altered), knapped chert, common charcoal and plant remains, and occasional phosphatic coprolitic grains. Some bones show partial dissolution features. Calcitic root casts have also been identified. The striking dark colour of this layer is due to the organic inputs from remains of combustion, namely charcoals and, to a lesser extent, burned bones. No intact combustion feature was identified during our excavations, but small domains of calcitic ashes can be observed in thin section (SI Fig. 4). The exact nature and versatility of human actions leading to the accumulation of Layer I are currently being studied. However, preliminary observations show a marked increase of anthropogenic input associated with combustion activities and abundance of bone splinters. Whereas the main deposition processes of Layer I relate to anthropogenic activities, the presence of crudely bedded lenses is also evident micromorphologically (typically 1.5 mm thick and reworking components of maximum 2 mm in size – see SI Fig. 6). This small-scale bedding is more abundant and the sediments are relatively better sorted in the Main Sector. Such bedding is syn-depositional and associated with low energy, unchanneled sheet wash that reworked exposed artefacts on a surface (SI Fig. 6). Such observations attest to site abandonment and elapsed time between – mainly anthropic – depositional events. The upper contact of Layer I with the Middle LU (Layers H and G) is sharp and relates to a shift in the main process of deposition.

Middle LU: Layers H and G

The Middle Lithostratigraphic Unit (Layers G and H) is ~50 cm thick water laid deposits composed of well-sorted lenses and laminae of sands, silts and clays. Variations in grain-size frequencies are caused by cyclic changes in sediment supply and sedimentation energy. The sedimentary source is from the interior of the karst system towards the entrance, as shown by the mild tilt in this direction of the deposits, ripped up papules, as well as the presence of bedded carnivore/omnivore coprolites. These deposits contain rare bones, and the ones present tend to come from the base of the unit, presumably material pulled up from the top of the underlying layers at the onset of sheet wash processes. This inference is clear in thin section where aggregates of darker materials, characteristic of Layer I, are attached to bone fragments (SI Fig. 8c). Archaeological density is low in the overlying layers – Upper LU –, with no evidence for bioturbation or downward percolation of archaeological material to the underlying deposits. Therefore, Layers G and H essentially seal the Lower LU (Layer K, J and I).

Supplementary Figures: Stratigraphy and Site Formation
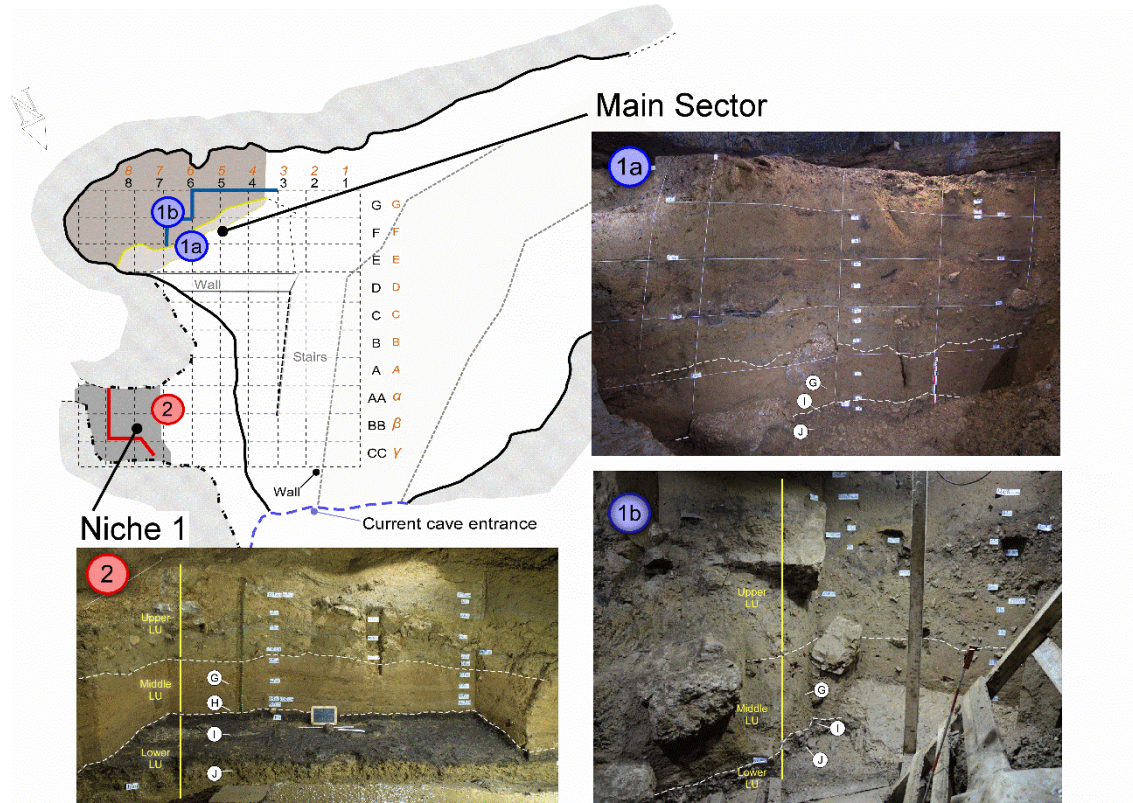
SI Figure 1: Map of Bacho Kiro Cave with current excavation grid in black and the grid system from the 1971-75 excavations[13] in orange. Field photographs show the stratigraphic sequence exposed in the Main Sector at the start of our excavations (1a), and during our 2018 field season in the Main Sector (1b) and in Niche 1 (2). Note the dark colour of Layer J, visible in the excavation surface in Niche 1 and at the bottom of the sequence in the Main Sector. Layer K had not yet been reached at this point of the excavations in the Niche 1 (see Extended Data Fig. 1).
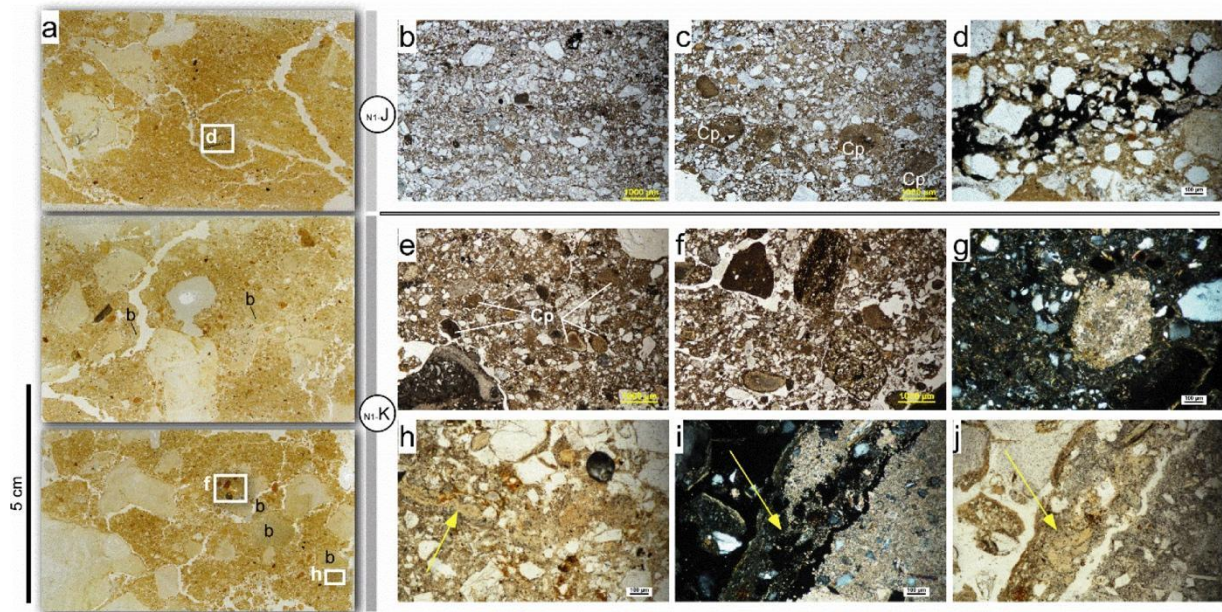
SI Figure 2: Layers K and J in thin sections from Niche 1 Sector. **a)** Thin section scans showing the coarser deposits of Layer K (two lower thin sections), with frequent limestone clasts, coprolite grains, and mm-sized bones ("b"). The upper thin section is the base of Layer J with relatively finer sediments, mainly sands and silts containing few bones. White boxes show the location of specific photomicrographs; **b)** Photomicrograph of crudely bedded silts and sands in Layer J, PPL, scale is 1 mm; **c)** Details of coprolite-rich ("Cp") lens in Layer J, PPL, scale is 1 mm; **d)** Band of manganese impregnating grains of quartz sand in Layer J, PPL, scale is 100 μm; **e)** Photomicrograph of Layer K. Note the coarser nature of the deposits with abundant coprolite grains, PPL, scale is 1 mm; **f)** Detail of coprolite and rounded siltstone granules in Layer K, PPL, scale is 1 mm; **g)** Decalcifying limestone and granostriated b-fabric typical of Layer K deposits in the Niche 1, XPL, scale is 100 μm; **h)** Phosphatic stringer (yellow arrow) in Layer K, PPL, scale is 100 μm; **i)** Detail of phosphatic rim on limestone fragment (yellow arrow) from Layer K, XPL, scale is 100 μm; **j)** Same as i) but in PPL.
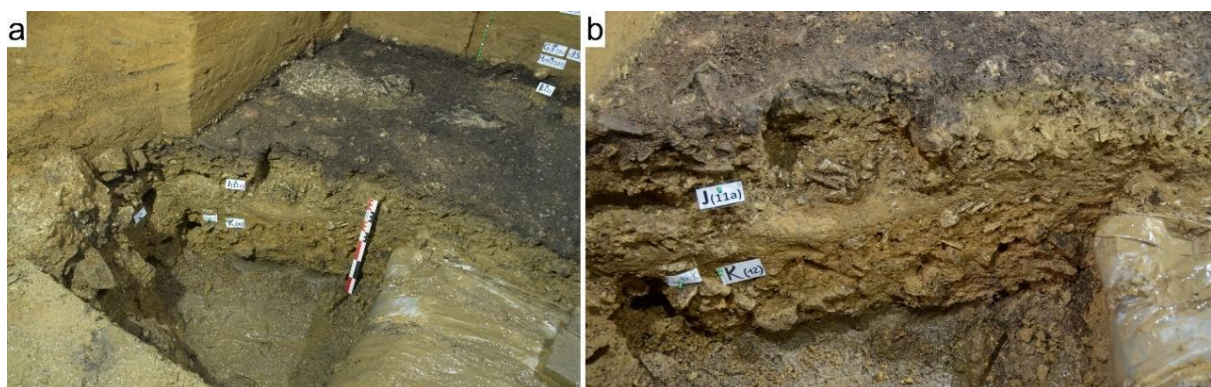
SI Figure 3: Lower Lithostratigraphic Unit in Niche 1. **a)** View of Layers K, J and I during excavation, scale is 50 cm; **b)** View of Layers I, J and K in profile. Note the sharp colour difference of Layer I above, the relatively finer deposits at the base of Layer J that increase in limestone clasts content towards its top.

7
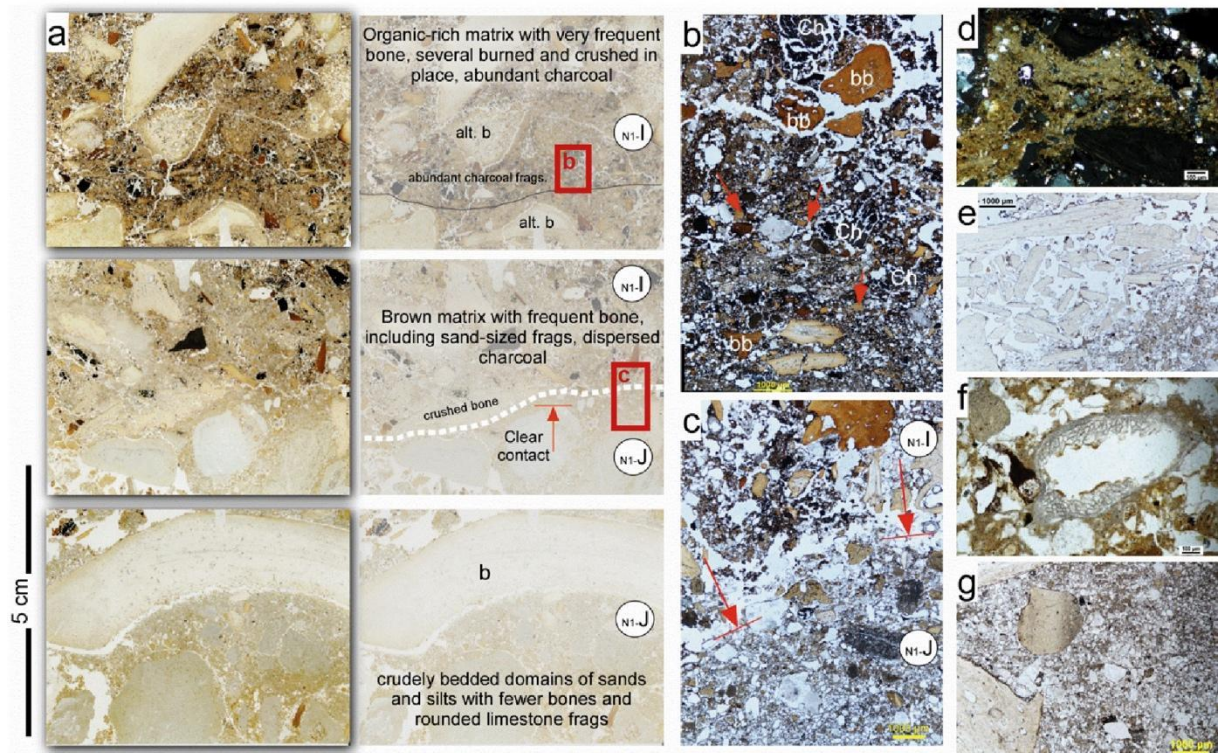
SI Figure 4: Contact between Layers J and I in the Niche 1. **a)** *Left* thin section scans with main micromorphological components and layer attribution drawn in the annotated thin sections to the *Right*. Note the clear contact between Layers J and I. Red boxes mark the location of specific photomicrographs. Alt. b. = altered bone; **b)** Composite of photomicrographs showing the organic-rich matrix of Layer I with common charcoals ("Ch"), bones, burned bones ("bb") and sand-sized bone fragments (red arrows). PPL, scale is 1 mm; **c)** Composite of photomicrographs of the contact between Layers J and I (arrows). Note the difference between the organic and bone-rich Layer I versus the siliciclastic brown matrix of Layer J below, PPL, scale is 1 mm; **d)** Photomicrograph of rare domain of calcitic ashes observed in Layer I, XPL, scale is 100 μm; **e)** In place crushed bone (possibly trampled) at the contact between Layers J and I, PPL, scale is 1 mm; **f)** Detail of rhizolith from Layer J, PPL, scale is 100 μm; **g)** Bone fragments, including rounded bone in siliciclastic deposits of Layer J that can be locally crudely bedded, PPL, scale is 1 mm.
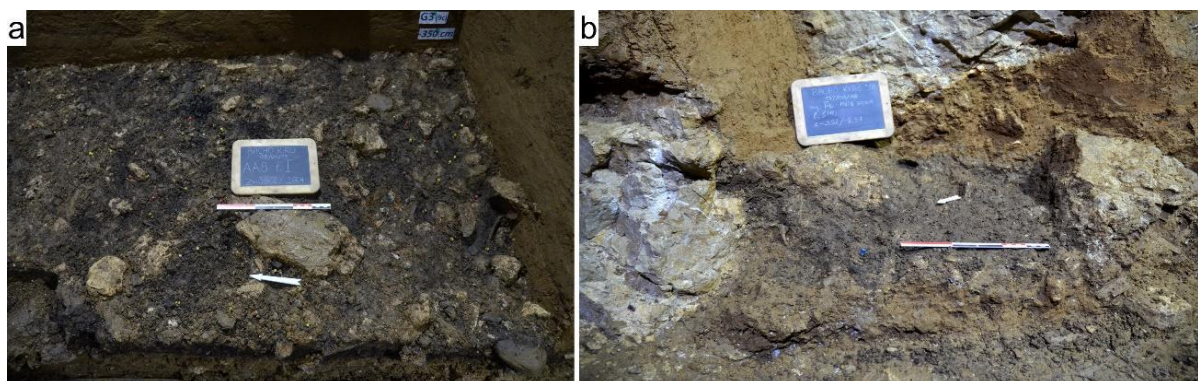
SI Figure 5: Field view of Layer I in the Niche 1 (a) and in the Main Sector (b). Note the distinct dark colour of this layer and the richness in archaeological material.
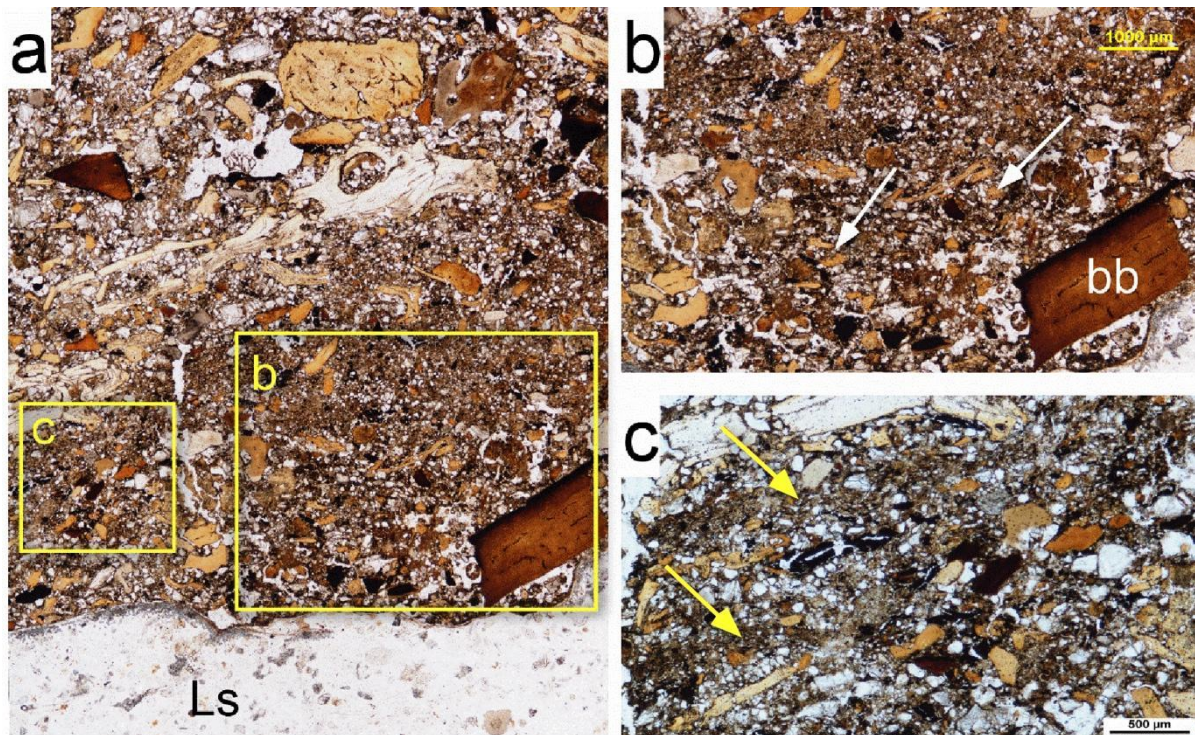
SI Figure 6: Detail of Layer I in thin sections. **a)** Large composite photomicrograph showing the abundance of bones, with crudely bedded lenses of sand-sized bone fragments. Yellow boxes show location of photomicrographs enlarged in b and c, "Ls" = limestone, PPL; **b)** Detail of laminae of silts, clay, and crudely bedded bones (white arrows show some examples). Note, however, the angularity of larger bone fragments, particularly burned bone ("bb"), PPL, scale is 1 mm; **c)** Detail of abundance of charcoals and bones interspersed with clayish silty crusts (yellow arrows), PPL, scale is 500 μm.
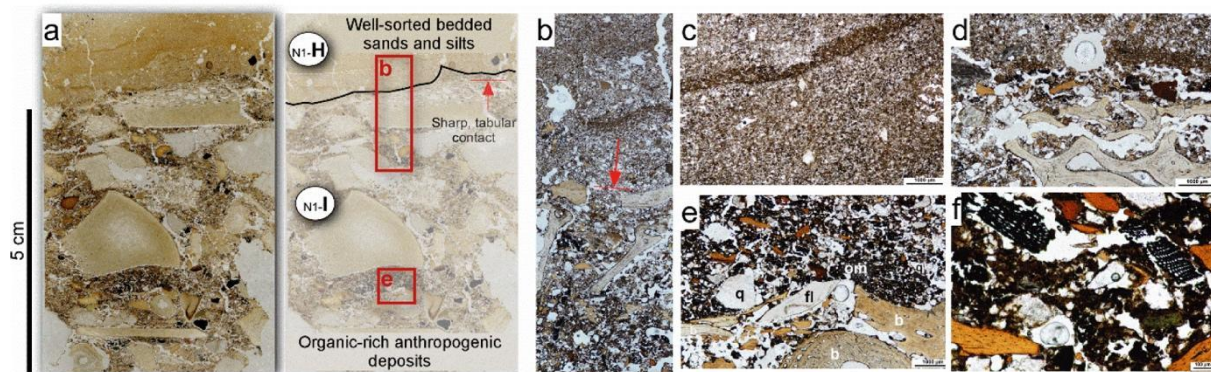
SI Figure 7: Contact between Layer I and H in the Niche 1 Sector. **a)** *Left* thin section scans and *right* annotated micromorphological characteristics and locations (red squares) of photomicrographs shown in b and e; **b)** Composite photomicrograph showing the sharp contact between bedded sands and silts of Layer H and the organic, bone-rich deposits of Layer I below (red arrow), PPL; **c)** Detail of well-sorted bedded laminae of Layer H, PPL, scale is 1 mm; **d)** Detailed view of the sharp contact between the Layer H (upper part of thin section) and I (lower part of thin section), PPL, scale is 1 mm; **e)** Photomicrograph of Layer I deposits with organic-rich matrix ("om"), bones ("b"), quartz ("q") and knapped flint ("fl"), PPL, scale is 1 mm; **f)** Detail view of organic-rich matrix with several charcoal fragments and sand-sized burned bones, PPL, scale is 100 μm.

9
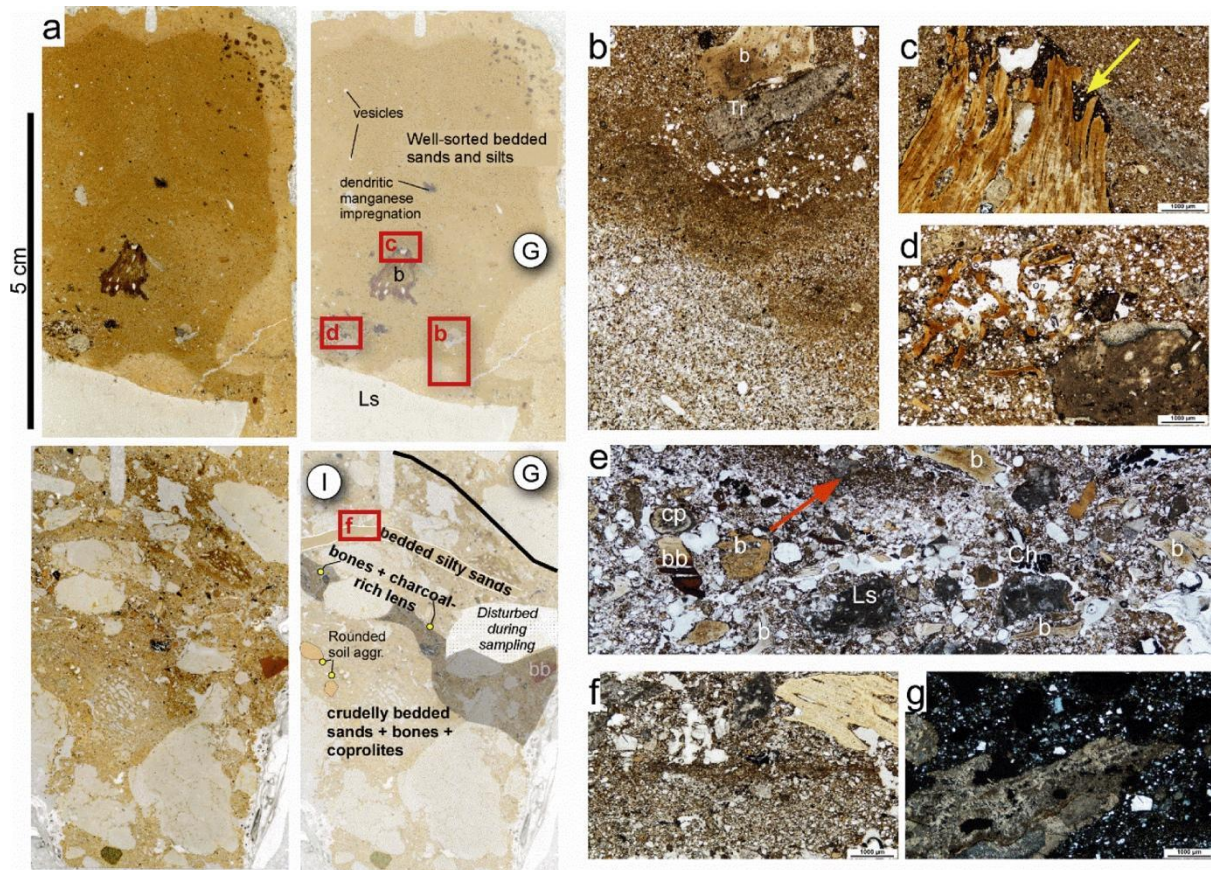
SI Figure 8: Contact between Layers I and G in the Main Sector; **a)** *Left* thin section scans and *right* annotated micromorphological characteristics and locations (red squares) of photomicrographs; **b)** Composite photomicrographs showing the well-sorted nature of Layer G water-laid deposits and the incorporation of rare bones ("b") and travertine fragment ("tr"), PPL; **c** and **d)** Detail of bones incorporated in the bedded sands of Layer G. These are interpreted as reworked from Layer I deposits, as evidenced from the darker, organic matrix surrounding these fragments (e.g. yellow arrow in c), PPL, scale is 1 mm; **e)** Composite photomicrograph of Layer I deposits with common bones (b), burned bones ("bb"), some coprolites ("cp") and rounded limestone granules ("Ls"). Note the bedded lens showing sheet wash deposition (red arrow), PPL; **f)** Detail of bedded silty sands lens within Layer I, scale is 1 mm, PPL; **g)** Decalcification of limestone fragment embedded in an undifferentiated b-fabric, XPL, scale is 1 mm.

Supplementary Tables

SI Table 1: Synthesis of the preliminary site formation processes inferred for the Lower and Middle LUs, their stratigraphic correlation between our two excavation sectors and correspondence with previous excavations at Bacho Kiro Cave[89].

LU	Layer Niche 1	Layer Main Sector	Main formation processes	Layers 1971-76 excavations
Middle	N1-G	G	*Main sedimentary sources:* reworked sands, silts and clays from inside karst system; Roof fall in the Main Sector.	9c -9a
	N1-H		*Main formation processes:* water laid deposits originating from inside the karst system.	10
Lower	N1-I	I	*Main sedimentary sources:* local contribution of limestone from spalling of cave roof and walls, substantial anthropogenic inputs; *Main formation processes:* debris from human occupation, with localized domains showing syn-depositional low-energy sheet wash. *Main post-depositional processes:* Some decalcification, small-scale bioturbation (namely roots).	11
	N1-J	J	*Main sedimentary sources:* local contribution of limestone from spalling, finer sediments reworked from inside karst system; *Main formation processes:* slope deposits with increasing human occupation towards top of layer; onset of syn-depositional low-energy sheet wash. *Main post-depositional processes:* Decalcification, small-scale bioturbation (namely roots).	11a
	N1-K	K	*Main sedimentary sources:* local contribution of limestone from spalling of cave roof and walls, finer sediments reworked from inside karst system; *Main formation processes:* slope deposits with sparse human occupation and abundant coprolite grains; *Main post-depositional processes:* Decalcification and rare domains of phosphatic accumulations, possibly from guano accumulations.	12

Supplementary Discussion 2: Lithics

Bacho Kiro Cave Layer 11 and the Initial Upper Palaeolithic:

The lithic assemblage from Layer 11 of the 1970s excavations at Bacho Kiro Cave[13] has been much debated. It was initially described as Upper Palaeolithic based on the presence of a "well developed" blade technology with typical Upper Palaeolithic techniques of blade production[94]. Retouched blades are the dominant type followed by retouched flakes, end-scrapers and splintered pieces with more rare occurrences of burins, truncations and notched pieces. It lacked, however, characteristic Aurignacian elements and so was therefore cautiously described as Pre-Aurignacian, given the name Bachokirian, and attributed to the earliest *Homo sapiens* in the Balkans[94]. The term Pre-Aurignacian was meant to emphasise that the assemblage had elements similar to or foreshadowing the subsequent Aurignacian and also that it represented an abrupt break from the preceding Middle Palaeolithic (in other words it was not a transitional industry which mixes Upper Palaeolithic elements into a Middle Palaeolithic base)[95]. This break is attested to in many ways including an abrupt shift in raw material usage (from coarse grained local volcanic rocks in the underlying Middle Palaeolithic at Bacho Kiro Cave to the use of imported, fine grain flints in Layer 11) to the near complete absence of Levallois technology[95]. At the same time, it was acknowledged[95] that it was not Aurignacian since it lacked typical carinated end-scrapers, carinated burins, Aurignacian blades, retouched bladelets of either Dufour or Krems type, and split-base bone points. This view, that Bacho Kiro Cave Layer 11 is not Aurignacian, is echoed by others who have examined the assemblage[96-98].

One of the main challenges to reconstructing the technology of the Bacho Kiro Cave Layer 11 assemblage has been the low number of cores (aside from core on flakes) and the intensive blade fragmentation. Thus, the technology of blade production is inferred only from a reading of the blades themselves, many of which have been fragmented, retouched into tools and/or reworked as cores. As the extensive refits at Boker Tachtit Level 1 showed[99], reconstructing the core reduction sequence from the blanks alone is challenging and subject to misinterpretation. Teyssandier[100] has argued that the few cores that are present in the Bacho Kiro assemblage are not related to the blade production and that the blades themselves are bi-directional and appear to come from larger, flatter surfaces than is typical of prismatic blade production. This along with the use of hard hammer direct percussion and platform faceting suggested to Teyssandier[100] a more Middle Palaeolithic character to the assemblage. Kozlowski[101], however, argued that the blades implied a rounding of the cores more typical of prismatic production.

At roughly the same time, there developed a growing appreciation that Bacho Kiro Cave Layer 11 shares strong similarities with industries from the Levant, like those of Boker Tachtit, that were

placed into an increasingly larger unit or techno-complex called the Initial Upper Palaeolithic or IUP[15,102]. At first, the Initial Upper Palaeolithic was used to describe the top of the Boker Tachtit sequence (Layer 4), which is characterised by the production of prismatic blades (normally an Upper Palaeolithic trait) through the use of hard hammer percussion with some platform faceting (normally both more characteristic of the Middle Palaeolithic)[2]. Typological Levallois blades and points exist in this assemblage from Boker Tachtit but the discarded cores do not show their production meaning that, contrary to what is argued for the Middle Palaeolithic, Levallois products were not the desired end-products of the technology. Later Kuhn et al.[103] expanded the definition of the Initial Upper Palaeolithic to include the lower layers from Boker Tachtit, which had previously been called Emiran, linked by Marks to the preceding Middle Palaeolithic. These authors[103] focused on the commonalities of prismatic blade reduction with the retention of Levallois features and ignored local variants (e.g. Emireh points). Once this generalisation is made, Bacho Kiro Cave Layer 11 falls within the Initial Upper Palaeolithic, and the Initial Upper Palaeolithic becomes a unit found across large expanses of Eurasia from Moravia to the Altai in the time window of roughly 45 - 39 ka[2].

Layer I (N1-I) from the new excavations:

Our excavations in the 2015-2018 seasons produced a new series of lithics from layers equivalent to Kozlowski's Layer 11. Most of our lithics come from Layer N1-I (n = 1,468) in the Niche 1. The few (n = 31) coming from the Main Sector have been combined (n = 1,499) with the Niche 1 in the description that follows (see Main Text Figure 1a for the location of the excavation sectors). Overall our new assemblage is entirely consistent with what has been previously described of Layer 11.

In terms of raw materials, the artefacts are primarily made on different types of allochthonous, fine-grained flint attributable to Lower Cretaceous (Aptian) and Upper Cretaceous (Campanian) limestone formations preferentially collected in sub-primary positions in the *alterites*. These source areas are between 150 km to the east and northeast and 80 km to the northwest of Bacho Kiro Cave. Approximately 14% of the artefacts from this layer show signs of burning, in keeping with the sedimentological observations of evidence for the intense presence of fire.

The assemblage consists of 260 blades, 554 flakes, 195 retouch flakes, 15 small cores, 327 tools, 15 core maintenance artefacts, and 105 pieces of debris. The tool to blank ratio is quite high (0.4), as is the blank to core ratio (76). Together these normally suggest intensive core reduction and tool production. However, in this case the very low quantities of manufacture debris (>20 mm) and the absence of by-products of reshaping blade cores are more suggestive of off-site production and the transport of finished products into the cave. Also consistent with this interpretation is the low percentage of cortex in the assemblage (88.3% with 0%, 4.8% with 1-50%, 3.9% with 50-99%,

and 3% with 100% cortical coverage). Consistent is also the frequent evidence for reworking in the form of resharpening through burination, bipolar reduction on anvil, and the use of flakes and blade fragments as cores. The large number of retouch flakes also testifies to tool manufacture or tool maintenance on site.

The blade technology combines aspects of Levallois with an Upper Palaeolithic blank production technology. The largest blades are up to 85 mm in length, 45 mm wide, and 15 mm thick (SI Fig. 9), and likely come from quite large cores (probably at least 12 cm in length based on the longest blades in the assemblage). The blank production technology is mostly unipolar parallel and less often bipolar, as shown by previous removal negatives on the blades (SI Tab. 2a). The flaking surfaces were likely flat and straight (like the largest blades in the assemblage). Platforms are mostly unprepared (plain), but nevertheless quite often facetted (SI Tab. 2b). Platform widths among blades are between 3 and 40 mm and thicknesses are between 5 and 30 mm. Exterior platform angles fall mostly between 85-90º. The frequent presence of prominent bulbs of percussion on blanks is consistent with direct hard hammer percussion. Medium-sized and small-sized blades are produced in continuity with the large blades. Where these are morphological bladelets, they are mostly unretouched. There is no evidence of intentional bladelet production from prismatic cores, with soft hammer percussion. Rather the bladelets are coming from re-sharpening tool edges, bipolar anvil flaking, core trimming, the thinning of flake scar ridges on thicker flakes and blades prior to their removal, etc.

The retouched tools represent approximately 30% of the lithic assemblage. Blades are the most common blank for tool production. In Layer I there are various pointed blades with combinations of Middle and Upper Palaeolithic techno-typological attributes (Extended Data Fig. 2 and Extended data Fig. 3: 1, 4, 6). The retouched pointed blades are morphologically and metrically diverse from large and straight symmetrical examples to more narrow and fine light blades (Extended Data Fig. 3: 2, 4), sometimes asymmetrical, with a bec (Extended Data Fig. 2: 3) or with a slightly oblique truncation (Extended Data Fig. 3: 1, 5, 7). The retouch is variable as well from large semi-covering retouch (Middle Palaeolithic type) to semi-abrupt and finer retouch covering only the distal part (Extended Data Fig. 3: 7). Some pointed blades exhibit macro-fractures (i.e. pseudo burin blows) (Extended Data Fig. 3: 4). The tools also include Upper Palaeolithic types like end-scrapers (SI Tab. 2c). Except for the points, which are mostly on blades, the various other tool types are equally made on blades and flakes.

While Layer I (and N1-I) from our excavations is clearly consistent with Layer 11 from the previous excavations and clearly Initial Upper Palaeolithic, it is less clear where the Initial Upper Palaeolithic begins in the sequence of Bacho Kiro Cave as well as where it ends. This is mainly due to the sometimes quite small sample sizes from Layer J below and the layers above Layer I (both in our

own excavations and in the previous ones). In general, material from Layers H, F, E, and D from our excavations or from equivalent layers from Kozlowski's excavation show a continuation of the Layer I technology and do not show clear evidence of Aurignacian-like assemblages. The latter is clearly present, however, in Layer B and probably begins in Layer C. This difference between Layers A, B and C (the upper LU) and Layers G, H, I, and J (the middle and lower LU) is also observed in the state of weathering and in raw material diversity. As for Layer J (and N1-J), the assemblage is generally consistent with Layer I, especially at the top of the layer. However, again, there are relatively few stone artefacts, and it is yet difficult to say whether the entire layer is consistent with the Initial Upper Palaeolithic.

Supplementary Table 2: Some technological and typological aspects of the Layer I assemblage.

a) Layer I/N1-I dorsal scar patterns (percents) by blank type.

	Blade	Flake
Unidirectional parallel	96.9	87.4
Unidirectional convergent	0	0.2
Bidirectional parallel	2.3	2.7
Bidirectional convergent	0.4	0
Centripetal	0	1.4
Multidirectional	0.4	8.2
N	259	485

b) Layer I/N1-I platforms (percents) by blank type.

	Blade	Flake
Cortical	0.6	2.5
Plain	56.2	56.2
Dihedral	0	2
Prepared	3.8	7.3
Facetted	8.1	4.6
Chapeau de gendarme	0	1
Linear	20	18.7
Punctiform	3.1	2
Smashed	0.6	1.8
Broken	7.5	3.8
N	160	395

c) Layer I/N1-I tool types (percents) by blank type.

	Blade	Flake
End-scraper	5	4.1
Levallois point	0	1
Mousterian Point	2.5	1
Notched	2.5	2.1
Perforator	1.2	1
Pointed Blade	30	0
Raclette	0	1
Retouched blade	56.2	1
Retouched flake	0	75.3
Side-scraper	0	1
Splinter	0	10.3
Tool fragment	2.5	2.1
N	80	97
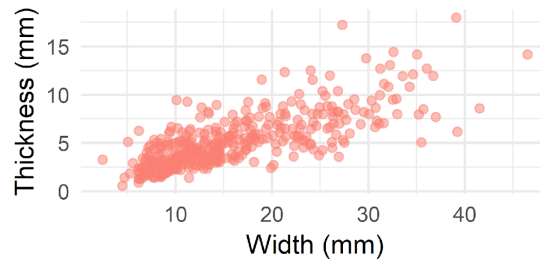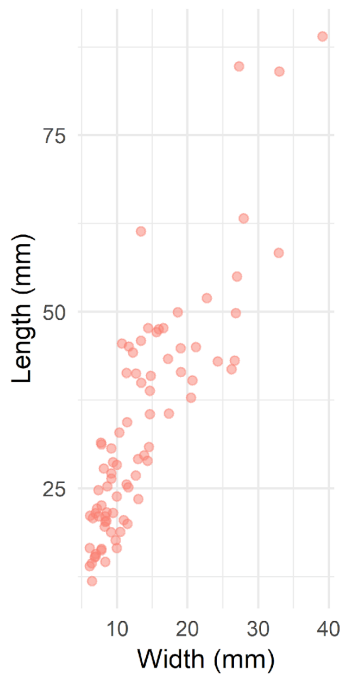
Supplementary Figure 9: Layer I blade shape. Length-width (left) based on complete blades only. Thickness-width (right) based on all blades.

Supplementary Discussion 3: Dental Morphology

The F6-620 M_2 crown is rectangular with a straight lingual outline commonly found in *H. sapiens* and contrasts with the convex lingual outline observed in Neanderthals[104]. The crown has four cusps that contact each other at the occlusal basin ("+" fissure pattern). The protoconid and metaconid have well developed essential crests that are divided by the sagittal sulcus, corresponding to the grade 1 of middle trigonid crest[105]; however, at the enamel dentine junction they join to form a low continuous crest that dips in the middle (grade 2) (Extended Data Fig. 4). The middle trigonid crest forms the distal border of a wide anterior fovea, and the mesial margin is low. The protostylid, deflecting wrinkle, cusp 6 and cusp 7 are absent.

The tooth is moderately worn: all four cusps are flattened and there is a single small dentine patch on the hypoconid grade 3[106]. A small chip of enamel is missing from the occlusal rim of the hypoconid and another enamel chip is missing just above the distal interproximal facet (IPF). The distal IPF is moderately sized (2.3 x 4.8 mm) and the mesial IPF is slightly larger (2.5 x 5.2 mm). The buccal and lingual grooves are shallow and wide. The buccal enamel border dips only slightly at the root bifurcation and no enamel extension is present[107]. The mesial and distal roots bifurcate approximately 3.5 mm from the enamel border and the pulp chamber is somewhat expanded. The roots are compressed and separated by a deep fissure for about two thirds their length until they fuse above the apices.

Supplementary Discussion 4: ZooMS Analysis

ZooMS screening was relatively successful, with 1213 samples (95.4%) being identified to some taxonomic level, 32 samples containing some collagen peptides that were insufficient even for broad taxonomic classifications, and 26 samples containing no suggestion of surviving collagen (SI Tab. 3). Among the fauna, Ursidae (27.7%) and *Bos/Bison* (42.3%) dominate in the Layer N1-I/Layer I, but there is a wide variety of other taxonomic groups present, including species represented by a small number of specimens, such as Rhinocerotidae (n=3). Among the 1271 screened specimens, we identified six hominins (Extended Data Fig. 5). These derive from the old excavation Layer 6a/7 (n=1), Main Section Layer B (n=1), and Niche 1 area Layer N1-I (n=4).

As for the isotopic data[4], deamidation analysis of collagen peptides P1105 and P1706 indicates well-preserved collagen in the entire dataset (SI Fig. 10a). We observe no relationship between bone specimen length and collagen deamidation (SI Fig. 10b), permitting further comparisons between subsamples and layers. These reveal that there might exist some differences in protein preservation between the Main Sector and Niche 1 areas for the same stratigraphic units (SI Fig. 10c), but that within a single layer at a single location there is large concordance between the deamidation distributions of different species (SI Fig. 10d). These observations further support previous notions that spatial patterns of glutamine deamidation exist within cave sites[45]. For Bacho Kiro Cave, hominin deamidation values, when available, fall within the range of deamidation values observed for stratigraphically associated samples (SI Fig. 10e, f). The hominins and fauna, therefore, do not differ in the extent of molecular diagenesis (deamidation) they experienced during deposition.

Supplementary Table 3: Table summarizing the identifications made by ZooMS. Counts are summed per layer in the Niche 1 and Main Sector areas, or by Kozlowski's[13] layer designations from the old collections available to study.

Barcode ID	no data	11	6a/7	A0	A1	A2	B	C	D	E	F	G	H/I	I	I/J	J	N1-3	N1-G	N1-H	N1-I	N1-I/J	N1-J	N1-K	Total
Elephantidae																						1	3	4
Equidae					1		4	6	1		4				2				1	83	1	2	7	112
Rhinocerotidae											5			2						1			4	12
Bos/Bison	1	1		1	15		10	12	5	2	4	5	1	23	19	3	3	1	1	325	1	5	38	476
Capra sp.						1	9	2	1				1	6	2					63		1	13	99
Sheep/Chamois														3	2	2				1	1		2	11
Cervid/Saiga						1	2	2		1	2			3	1					6		3	13	34
Rangifer					4																			4
Roe deer					1																			1
Homininae			1				1													4				6
Felinae																						1		1
Red fox				2																				2
Ursidae	1	5	1		8	1	20	15	7	6	13		1	40	50	2	3	1	2	188		9	20	393
Artiodactyla							1													2				3
Bovidae					1																			1
Bovidae/Cervidae					1															1				2
Bovidae/Reindeer							1	1												2				4
Bos/Bison/Muskox					4										1					3				8
Sheep/Chamois/ *Capra* sp.					1		1							1						1			2	6
Capra sp./Reindeer							2													9				11
Cervid/Saiga/Roe deer																				2			1	4
Carnivora/Bovidae																	1							1
Carnivora								1												2				3
Felidae/Mustelidae																				1				1
Pantherinae/Hyaenidae																				5			1	6
Pantherinae/Mustelidae									1					1										2
Ursidae/Felinae							1	1												4				6
Unidentifiable					3		1	2						3	1		1		2	18		1		32
Empty		1			2		1										3			19				26
Total	**2**	**7**	**2**	**3**	**41**	**3**	**54**	**42**	**15**	**10**	**28**	**5**	**3**	**82**	**78**	**7**	**11**	**2**	**6**	**740**	**3**	**22**	**105**	**1271**
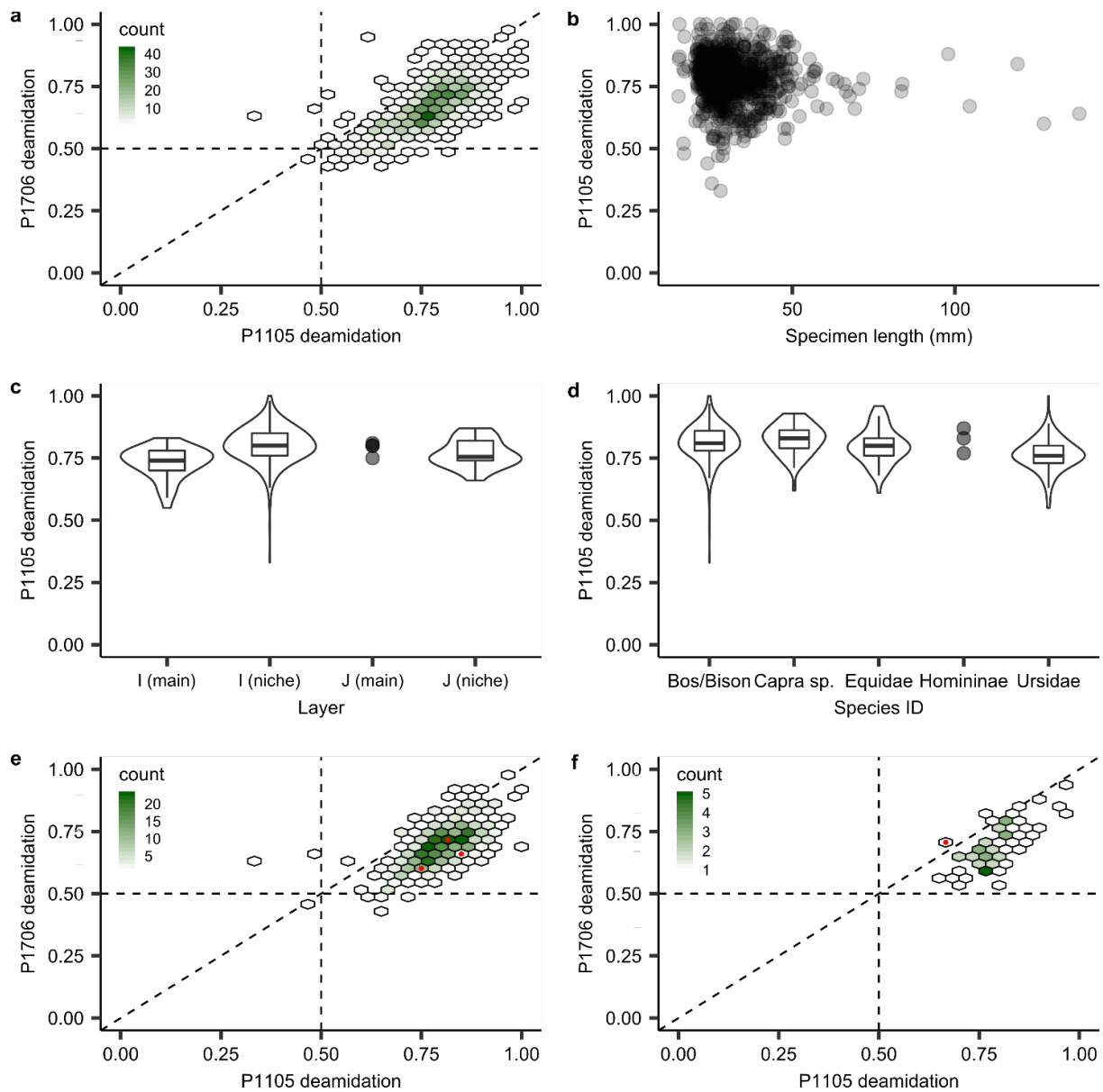
Supplementary Figure 10: Glutamine deamidation in the Bacho Kiro Cave ZooMS dataset. a, Relationship between P1105 and P1706 deamidation (n = 882). b, Relationship between bone specimen length and P1105 deamidation (n = 879). Each point represents a single specimen. c, Violins and boxplots of P1105 deamidation for Layers I and J in respectively the Main Sector and Niche 1 areas. d, Variation in P1105 deamidation between five different taxa present in Layers N1-I and I. For c and d, boxplots show the mean, 25th/75th quartiles, and 1.5 times the interquartile range. e, Deamidation of P1105 and P1706 for Layers N1-I, I, and 11, with hominin values highlighted in red (n = 491). f, Deamidation of P1105 and P1706 for Layers B, C, and 6a/7, with hominin values highlighted in red (n = 62). All comparisons only based on deamidation measured using the ammonium-bicarbonate extraction protocol. 1=no deamidation, 0=complete deamidation of the single glutamine present in the peptides P1105 and P1706.

Supplementary Discussion 5: Palaeogenetics

General characteristics of DNA libraries

The number of unique DNA molecules was estimated at between 2.8×10^8 and 7.8×10^9 for each sample library (SI Tab. 4) and was thus higher than the extraction and library negative controls (SI Tab. 5). Between 272,052 and 919,463 reads (SI Tab. 4) were obtained following sequencing on a MiSeq (Illumina). After discarding fragments shorter than 35 bp, between 13,856 and 795,043 unique mtDNA fragments with a mapping quality of at least 25 were recovered from seven Bacho Kiro Cave specimens (SI Tab. 4), resulting in an average coverage of between 55 and 2,629-fold.

Authentication of DNA fragments

Elevated frequencies of C-to-T substitutions almost always occur in authentic ancient DNA due to deamination of cytosines (C) to uracils (U), particularly towards ends of DNA fragments[111], and are predominantly absent in present-day contamination[73,109]. Among the mtDNA fragments from the Bacho Kiro Cave specimens, C-to-T substitutions ranged from 13.5% to 54.9% at 5'-ends and from 9.4% to 42.2% at 3'-ends of molecules, respectively (Extended Data Fig. 6). For the libraries from specimen F6-597, these frequencies increased substantially when filtering for the fragments that carry a C-to-T substitution at the opposing ends ('conditional substitutions', see Extended Data Fig. 6), indicating that both endogenous ancient DNA as well as present-day human DNA contamination are present in this specimen[69]. For all the other specimens, C-to-T substitution frequencies remained stable after filtering for the presence of C-to-T substitutions at the opposing ends, suggesting that they are much less contaminated with present-day human DNA.

MtDNA sequence reconstruction, haplogroups and phylogenetic inferences

We reconstructed full mtDNAs of the Bacho Kiro Cave molar (F6-620), as well as of the specimens AA7-738, BB7-240, CC7-2289, CC7-335 and BK-1653, first using all mapped mtDNA fragments longer than 35 base pairs with a mapping quality of at least 25, and second using only fragments with a C-to-T difference to the reference genome at the first three and/or last three terminal positions. For each of these specimens the reconstructed mitochondrial genomes from all fragments and from putatively deaminated fragments were identical. Moreover, the mitochondrial genomes of the Bacho Kiro Cave molar (F6-620) and the specimen AA7-738 were indistinguishable from one another, suggesting that they could come from the same or maternally related individuals.

The reconstructed mtDNAs of Bacho Kiro Cave specimens were aligned to 54 present-day humans, 12 ancient *H. sapiens* (SI Tab. 9), 22 Neanderthals, four Denisovans, one Sima de los Huesos individual and a chimpanzee to determine to which hominin group they belong. All of the six Bacho Kiro Cave mitochondrial genomes fall within the variation of *H. sapiens*. The haplogroups of the reconstructed mtDNAs were identified using HaploGrep[87] and the Phylotree database (build 17). Bacho Kiro Cave molar (F6-620) and specimen AA7-738 carry the substitutions that define the M haplogroup with 0.98 posterior support (73G, 263G, 489C, 750G, 1438G, 2706G, 4769G, 7028T, 8701G, 8860G, 9540C, 10398G, 10400T, 10873C, 11719A, 12705T, 14766T, 14783C, 15043A, 15301A, 15326G, 16223T), along with two substitutions (4730T and 5315G) not seen in any present-day human population. The specimens BB7-240 and CC7-335 carry the substitutions characteristic of the N haplogroup (73G, 263G, 750G, 1438G, 2706G, 4769G, 7028T, 8860G, 9456G, 11719A, 12705T, 14766T, 15326G, 16223T) with 0.93 and 0.92 posterior support, respectively. Both of them share two mutations (4113A, 8155A) not detected in any present-day human population along with one specific mutation for each of them (194T in BB7-240 and 14790G in CC7-335) and fall basal to the other individuals of the macrohaplogroup N, with the smallest number of differences to Oase1[36]. Specimen CC7-2289 carries the substitutions defining the R haplogroup (73G, 263G, 750G, 1438G, 2706G, 4769G, 7028T, 8860G, 11719A, 14766T, 15326G) with no private mutations and no additional substitutions that define sub-clades of haplogroup R, suggesting a relationship to the mtDNA ancestral to present-day haplogroup R. The mitochondrial genome of the specimen BK-1653 belongs to haplogroup U8, commonly found in other Upper Palaeolithic humans in Europe[29,110], and shows the smallest number of differences to the mtDNA genome of Kostenki 14[73].

We were unable to reconstruct a full mitochondrial genome of specimen F6-597 from deaminated fragments only, and the conditional substitutions as well as the contamination estimates suggested that substantial present-day human DNA contamination is present in this specimen in the addition to endogenous ancient DNA. In order to determine to which hominin group F6-597 belonged, we investigated the state of fragments overlapping 'diagnostic' positions specific for the branches in the mtDNA tree relating present-day humans, Neanderthals, Denisovan and the hominin from Sima de los Huesos[68] (SI Tab. 6). Out of all fragments overlapping these positions, between 99.4% and 99.9% matched the modern human state (SI Tab. 6). After restricting our analyses to putatively deaminated fragments, 100% of the fragments supported the modern human state, irrespective of the panel of diagnostic sites used (SI Tab. 6). The observed fragments (between one and four) supporting other states when using all fragments likely stem from sequencing errors. Therefore, we conclude that the specimen F6-597 had a mitochondrial genome of a *H. sapiens*-type.

Present-day human DNA contamination estimates

We identified two positions where the mitochondrial genomes of Bacho Kiro Cave molar F6-620 and specimen AA7-738 differ from at least 99% of a world-wide panel of 311 present-day humans. Three such positions were identified for specimens BB7-240 and BK-1653 and four for specimen CC7-335 (SI Tab. 7). We did not detect any positions where the specimen CC7-2289 would differ from 99% of 311 present-day humans. We then used fragments overlapping positions that are 'diagnostic' for each specimen to estimate the levels of present-day human DNA contamination among all fragments and putatively deaminated fragments only (SI Tab. 8). The proportion of fragments matching the present-day human state ranged from 0.2% to 2.9% among all fragments, and between 0% and 1.6% among putatively deaminated fragments.

Using schmutzi[88] we estimated the proportion of present-day human DNA contamination among all fragments of specimen F6-597 to be 63.5% (95% confidence intervals (CI): 62.5-64.5%) and 1% (95% CI: 0-2.0%) among all fragments of specimen CC7-2289. After restricting the analyses to putatively deaminated fragments, estimates of present-day human DNA contamination for the specimens F6-597 and CC7-2289 were 1% (95% CI:0-2.0%) and 0% (95% CI:0-0.05%), respectively.

Molecular DNA dating

The tip dates for the Bacho Kiro Cave specimens were estimated in a Bayesian framework implemented in BEAST2[89] by using 10 securely radiocarbon dated ancient *H. sapiens*[28,29,71-73], 54 present-day humans[69] and Vindija 33.16 Neanderthal genome as an outgroup[69]. We used Tamura-Nei 93 with a fixed fraction of invariable sites and gamma distributed rates (TN93+I+G) as the best-supported model for this dataset as determined with jModelTest2[90]. Following a marginal likelihood estimation (MLE)[91] analysis for model comparison and best support assessment, we determined the relaxed clock model and constant population size to be the best fit to the data. We estimated the tip dates of the Bacho Kiro Cave specimens from Layer I to range between 44,830 (95% highest posterior density (HPD): 32,534-57,017) and 42,616 (95% HPD: 29,946-54,246) years before present (BP) (Extended Data Tab. 2). For BK-1653 from Layer B we estimated the tip date to be 30,763 (95% HPD: 20,602-39,544) years BP (Extended Data Tab.2).

Supplementary Table 4: Characteristics of DNA libraries prepared from the Bacho Kiro Cave specimens.

Specimen	Amount of powder (mg)	Extract ID	Library ID	Number of molecules (qPCR)	Number of control oligonucleotide (qPCR)	Number of fragments generated	Number of unique mtDNA fragments ≥ 35bp, MQ≥25	Average number of duplicates	Number of fragments with C→T substitution ≥ 35bp, MQ≥25
Molar (F6-620)	29.3	E9293	A11197	3.18E+10	1.11E+06	784,156	283,189	1.46	101,149
			A12357	2.05E+10	1.42E+06	398,173	134,157	1.25	42,403
			A12550	1.48E+10	8.29E+05	434,132	148,547	1.32	48,085
			A12944	1.74E+10	9.93E+05	351,797	127,368	1.24	37,124
			A15716	2.86E+10	1.44E+06	344,530	101,782	1.27	28,527
AA7-738	30.4	E9294	A11198	2.84E+09	1.07E+06	919,463	14,669	29.99	4,382
			A12358	4.58E+09	1.34E+06	402,522	16,480	8.19	4,678
			A12554	4.05E+09	7.37E+05	369,910	15,177	8.51	4,300
			A12945	5.88E+09	1.12E+06	318,168	17,823	6.37	4,907
			A15717	5.06E+09	9.95E+05	371,184	8,525	10.51	2,232
BB7-240	32.1	E9295	A11199	1.35E+10	2.21E+05	908,778	113,820	3.79	43,812
			A12359	8.39E+09	2.09E+05	455,891	81,545	2.01	30,660
			A12555	7.90E+09	1.82E+05	322,514	67,633	1.71	24,400
			A12946	1.32E+10	2.80E+05	306,486	73,047	1.57	26,105
			A15718	1.72E+10	3.12E+05	367,713	54,338	1.98	19,404
CC7-2289	34.3	E9296	A11200	5.60E+10	5.69E+05	876,425	12,054	29.37	3,941
			A12360	2.70E+10	9.17E+05	347,523	12,656	6.14	3,594
			A12556	2.12E+10	5.03E+05	275,362	11,036	5.90	3,092
			A12947	3.45E+10	7.84E+05	272,052	12,558	4.82	3,600
			A15719	3.56E+10	6.20E+05	374,203	6,168	6.72	1,707
CC7-335	52.4	E9297	A11201	3.07E+09	9.20E+05	848,726	117,489	3.55	43,016
			A12361	4.17E+09	1.62E+06	413,039	89,555	1.83	30,394
			A12557	2.81E+09	7.00E+05	339,537	79,249	1.70	25,745
			A12948	4.45E+09	1.15E+06	284,541	72,185	1.61	23,775
			A15720	6.90E+09	1.31E+06	392,825	65,879	2.06	21,443
F6-597	45.6	E9298	A11202	7.75E+10	7.46E+05	762,226	2,915	45.44	312
			A12362	4.76E+10	1.27E+06	374,517	3,349	8.26	289
			A12558	4.21E+10	6.55E+05	339,783	2,949	6.51	279
			A12949	4.89E+10	1.06E+06	274,627	3,228	5.14	293
			A15721	6.44E+10	1.04E+06	349,202	1,415	6.37	87
BK-1653	64.7	E9299	A11203	2.44E+10	8.28E+05	806,497	159,260	2.60	28,427
			A12363	2.14E+10	1.47E+06	400,870	101,873	1.52	16,207
			A12562	1.63E+10	9.64E+05	324,409	87,822	1.43	14,498
			A12950	1.93E+10	1.01E+06	308,927	87,996	1.42	13,310
			A15722	3.06E+10	1.13E+06	328,346	63,244	1.56	10,631

qPCR – quantitative PCR; C→T – cytosine to thymine

Supplementary Table 5: Characteristics of extraction and library negative controls.

Negative control	Library ID	Number of molecules (qPCR)	Number of control oligonucleotide (qPCR)	Number of fragments generated	Number of unique mtDNA fragments ≥ 35bp, MQ≥25	Average number of duplicates	Number of fragments with C→T substitution ≥ 35bp, MQ≥25
Extraction negative control	A11205	1.43E+07	1.06E+06	116,648	179	295.7	5
Library negative control	A11427	5.96E+07	6.82E+05	87,654	59	434.27	2
Library negative control	A12377	6.21E+07	1.51E+06	69,937	515	44.34	3
Library negative control	A12575	2.93E+07	8.08E+05	45,805	30	417.1	2
Library negative control	A12965	4.60E+07	7.67E+05	55,178	134	133.55	2
Library negative control	A15705	1.52E+08	9.58E+05	30,127	11	102.09	-

qPCR – quantitative PCR; C→T – cytosine to thymine

Supplementary Table 6: MtDNA fragments from Bacho Kiro Cave F6-597 matching the extant *H. sapiens* state using three sets of diagnostic positions. All fragments and putatively deaminated fragments overlapping three panels of positions diagnostic for each branch in the mtDNA tree relating present-day humans, Neanderthals, Denisovans, one hominin from Sima de los Huesos and a chimpanzee. The number of fragments supporting the given state and the total number of fragments are given in brackets.

	Panel 1		Panel 2		Panel 3	
	Present-day human %	Neanderthal/Denisovan /Sima/Chimp %	Neanderthal %	Human/Denisovan/ Sima/Chimp %	Denisovan %	Human/Neanderthal/ Sima/Chimp %
All fragments	99.36 [618/622]	0.04 [4/622]	0.15 [1/684]	99.85 [683/684]	0.08 [1/1,256]	99.84 [1,255/1,256]
Deaminated fragmens	100 [37/37]	0 [0/37]	0 [0/50]	100 [50/50]	0 [0/80]	100 [80/80]

Supplementary Table 7: Positions 'diagnostic' for each of the reconstructed Bacho Kiro Cave mtDNAs. Positions that differ between each of the reconstructed mitochondrial genomes and 99% of a world-wide panel of 311 present-day humans[69].

Specimen	rCRS position	Base characteristic for the specimen	Base in 99% of 311 present-day humans
Molar (F6-620) and AA7-738	4730	T	C
	5315	G	A
BB7-240	4113	A	G
	8155	A	G
	9456	G	A
CC7-335	4113	A	G
	8155	A	G
	9456	G	A
	14790	G	A
BK-1653	2483	C	T
	6317	T	C
	9833	C	T

Supplementary Table 8: Present-day human DNA contamination estimates. Proportion of fragments overlapping positions that differ between each of the reconstructed mitochondrial genomes and 99% of a world-wide panel of 311 present-day humans[68]. The number of fragments supporting the given state and the total number of fragments are given in brackets.

Specimen	mtDNA fragments	Diagnostic positions	
		% Matching the specimen	% Matching 99% of 311 present-day humans
Molar (F6-620)	All	99.81 [2,630/2,635]	0.19 [5/2,635]
	Deaminated	99.88 [863/864]	0.12 [1/864]
AA7-738	All	99.25 [264/266]	0.75 [2/266]
	Deaminated	98.41 [62/63]	1.59 [1/63]
BB7-240	All	97.09 [1,633/1,689]	2.91 [49/1682]
	Deaminated	99.57 [693/696]	0.43 [3/696]
CC7-335	All	99.58 [1883/1891]	0.42 [8/1891]
	Deaminated	100 [779/779]	0 [0/779]
BK-1653	All	98.37 [2,356/2,395]	1.63 [39/2,395]
	Deaminated	98.86 [260/263]	1.14 [3/263]

Supplementary Table 9: Mitochondrial genomes of ancient _H. sapiens_, their respective geographical locations and radiocarbon dates that were used for phylogenetic analyses. All radiocarbon dates were calibrated using IntCal13 and OxCal v4.3.

	Geographical location				Radiocarbon date (calBP)		
Individual	Country	Lat.	Long.	mtDNA accession no.	Point estimate	95.4% confidence interval	Publication of the date
Ust'Ishim	Russia	57.43	71.1	-	45,020	42,560 – 47,480	[28]
Oase 1	Romania	45.12	21.90	-	39,580	37,310 – 41,760	[77]
Fumane 2	Italy	54.59	10.90	KP718913	39,805	38,500 – 41,110	[70]
Tianyuan	China	39.66	115.87	KC417443	39,008	37,761 – 40,254	[25]
Kostenki 14	Russia	51.23	39.3	FN600416	37,470	36,260 – 38,680	[73]
Dolní Věstonice 13	Czech Republic	48.53	16.39	KC521459	30,870	30,670 – 31,070	[27]
Dolní Věstonice 14	Czech Republic	48.53	16.39	KC521458	30,870	30,670 – 31,070	[27]
Oberkassel 998	Germany	51.23	6.75	KC521457	14,130	13,758 – 14,501	[27]
BS11	China	36.48	117.83	KC521454	8,050	7,940 – 8,160	[27]
Loschbour	Luxembourg	47.70	6.24	KC521455	8,050	7,940 – 8,160	[27]
Iceman	Italy	46.77	10.83	EU810403	5,191	5,067 – 5,315	[71]
Saqqaq Eskimo	Greenland	69.24	-53.54	EU725621	4,504	4,423 – 4,585	[72]

Supplementary Discussion 6: Macro Fauna, Small Mammals and Osseous Objects

New excavations at Bacho Kiro Cave have recovered a large quantity of piece plotted faunal material (>20 mm) from Layers I and J from both the Niche 1 (n=10,960) and the Main Sector (n=299). Current analysis of faunal material has focused predominantly on piece plotted remains from Layers I and J from the Niche 1 excavation row 7 (AA7, BB7, CC7) and also Main Sector (which are here combined and noted as Layer I and J respectively). The faunal reference collection stored at the Bulgarian National Museum of Natural History was used to accurately identify species and skeletal element. In order to locate and identify specific bone surface modifications (cut marks, impact points, percussion notches, carnivore tooth pits etc.), all material was studied under a 20x magnification hand lens and high power digital microscope (DinoLite), as required, using an oblique light source following previous protocols[111-117]. The worked artefacts, including bone tools and pendants, were studied using a Nikon SMZ 1000 stereomicroscope with a magnification range of 8x to 80x following previous protocols[118-121].

Faunal remains from the new excavations of Layers I and J include 23 species dominated by *Bos/Bison* (either *Bos primigenius* or *Bison priscus*), cervids (especially *Cervus elaphus*) and caprines (especially *Capra ibex*), alongside equids (*Equus ferus* and *Equus hydruntinus*) (SI Tab. 10). A diversity of carnivore species are present including cave bear (*Ursus spelaeus*) and less frequently canids (*Canis lupus, Cuon alpinus, Vulpes vulpes*), felids (*Panthera leo spelaea, Panthera pardus*) and cave hyaena (*Crocuta crocuta spelaea*). This faunal spectrum is characteristic of the biostratigraphic zone Mammal Neogene Quaternary (MNQ) 26[30,31] and is internally consistent across Niche 1 and the Main Sector, which correlates with both previous excavations[13] and ZooMS identifications (SI 4).

Fauna from Layers I and J contain species from the Mammuthus-Coelodonta Faunal Complex including woolly mammoth (*Mammuthus primigenius*), giant dear (*Megaloceros giganteus*), reindeer *(Rangifer tarandus)* and wolverine (*Gulo golo*)[122]. A complete reindeer phalanx was securely identified from Layer J, while wolverine (*Gulo gulo*) has never been identified in Pleistocene faunal assemblages from the Balkans. Both species were previously identified only at higher latitudes throughout central and western Europe, significantly further north than the eastern Balkans. This is indicative of a substantially colder climate than present day with wolverine, in particular, adapted to extremely cold climates.

The identification and analysis of bone remains recovered from the screened materials from all layers at Bacho Kiro Cave is ongoing. Currently, a small assemblage (n=287) of rodent remains from Layer J have been identified consisting mainly of isolated teeth. The remains are dominated by *Microtusex gr. arvalis-agrestis* (20.4%), *Chionomys nivalis* (14.2%), and *Terricola grafi* (9.7%). These species are frequently found in open and rocky habitats, though the relative proportion of the steppic species *Mesocricetus newtoni* (10.6%) is also significant. Less common are *Arvicola amphibious* (5.3%), N*annospalax leucodon* (4.4%), *Myodes glareolus* (2.7%), *Cricetulus migratorius* (2.7%), *Apodemus sp*. (0.9%), and *Sicista subtilis* (0.9%). Overall, the structure of the assemblage indicates the predominance of open habitats - meadows and steppes in a relatively cooler climate compared to present day. Such assemblages are typical of the semi-mountainous landscapes found in Late Pleistocene deposits of northern Bulgaria[123].

During the last ice age the climate of the Balkans was considered to be warmer than that of central and western Europe[13,124]. This mix of macro mammal species suggests shifts between warmer and colder climates at a more local or even regional scale than previously considered. Bacho Kiro Cave is situated in a semi-mountainous area with rugged terrain, a natural habitat for various caprines species (including *Rupicapra rupicapra* and *Capra ibex*). The cave was also situated close to both forested (illustrated by remains of wild auroch (*Bos primigenius*), felids (*Panthera pardus*) and canids) or mixed environments and to the north, steppic environments (exemplified by remains of horse (*Equus ferus*) and steppe bison (*Bison priscus*)). In combination, both the macro and micro-mammal assemblages from Bacho Kiro Cave illustrate that the Late Pleistocene climate around Bacho Kiro Cave was cooler than present day with a mix of environmental conditions at both a local and broad regional scale.

Faunal material from Layers I and J exhibit excellent preservation as illustrated by a low degree of sub-aerial weathering (stages 0-2; I: 92.8%; J: 96.5%) and a high degree of readability of bone surfaces (>50% readable I: 85.3%; J: 85.5%), permitting the identification of both carnivore and human bone surface modifications. Burnt bone was recorded following Stiner et al.[125], though very few burnt remains have been recovered (0.6%; n=19) in contrast to the proportion of burnt lithics from these levels. Despite the identification of carnivores within the Layer I and J fauna, there is no strong signal of carnivore activity on the bones for either Layer I (n= 57; 1.8%) or Layer J (n= 6; 2.4%) (SI Tab. 4).

A large range of anthropogenic modifications have been identified in both Layer I (n = 508; 16.5%) and Layer J (n = 16; 6.4%) and across both carnivore and herbivore taxa including skinning marks, cut marks, scraping marks and deliberate marrow fractures (see SI Tab. 5). Skinning

marks on carnivores could reflect the exploitation of such taxa for furs, though the use of these species for additional nutritional purposes cannot be excluded based on the current faunal data. Human modification across various herbivore species and elements illustrate all stages of the butchery sequence. This includes the skinning and disarticulation of the axial and appendicular skeleton along with cut marks that illustrate the filleting and removal of meat from limb bones. Further analyses of skeletal part indices are necessary to understand more fully the transport and subsistence decisions of human groups in Layers I and J.

The extraction of bone marrow from long bone shafts is illustrated by the occurrence of anvil and percussion marks (4.1%; n=136) on both carnivore and herbivore species. The fragmented bone assemblage has also been reused for informal (retouchers; n= 40) and more formal osseous artefacts (SI Tab. 5 and 6). Both categories have been produced on skeletal elements of both carnivore and herbivore species, including cave bear and *Bos/Bison* specimens and, in general, these follow the overall pattern of species abundance within Layers I and J (SI Tab. 1). Several pendants and a bead were also recovered from the IUP layers (SI Tab. 6). The more formal bone tools, pendants and the bead are similar to those from so-called transitional assemblages[4, 8,127,128] and artefacts recovered at other IUP sites[32,129] though further analyses will demonstrate whether or not production methods are similar. The bone tools documented from the new excavations at Bacho Kiro Cave are similar to those recovered from previous excavations of Level 11 and 11a (Layers I and J)[13,1130].

Supplementary Table 10: Analysed faunal material from Layers I and J from both Niche 1 and Main Sector

Scientific name	Common name	I	%	J	%	Total	%
	fish unknown	1	0,03	0	0	1	0,03
	bird unknown	2	0,06	0	0	2	0,06
	Leporid sp.	4	0,13	0	0	4	0,12
Carnivores							
Canis lupus	wolf	8	0,26	4	1,6	12	0,36
	Canis sp.	5	0,16	0	0	5	0,15
Cuon alpinus	dhole	0	0	1	0,4	1	0,03
Vulpes vulpes	red fox	3	0,1	1	0,4	4	0,12
Crocuta crocuta spelaea	cave hyaena	17	0,55	3	1,2	20	0,6
	Hyaena sp.	2	0,06	3	1,2	5	0,15
Gulo Gulo	wolverine	1	0,03	1	0,4	2	0,06
Panthera leo spelaea	cave lion	5	0,16	0	0	5	0,15
Panthera pardus	leopard	1	0,03	0	0	1	0,03
	Felidae sp.	0	0	1	0,4	1	0,03
Ursus spelaeus	cave bear	154	4,99	84	33,6	238	7,14
Ursus arctos	brown bear	3	0,1	2	0,8	5	0,15
	Ursus sp.	74	2,4	28	11,2	102	3,06
Herbivores							
	Rhino sp.	2	0,06	0	0	2	0,06
Equus ferus	horse	17	0,55	4	1,6	21	0,63
Equus hydruntinus	European ass	5	0,16	1	0,4	6	0,18
	Equid sp.	49	1,59	3	1,2	52	1,56
Bison priscus	steppe bison	14	0,45	3	1,2	17	0,51
Bos primigenius	auroch	56	1,82	4	1,6	60	1,8
	Bos/Bison sp.	203	6,58	14	5,6	217	6,51
Capra ibex	ibex	33	1,07	3	1,2	36	1,08
Capra caucasica	west caucasian tur	10	0,32	0	0	10	0,3
Rupicapra rupicapra	chamois	1	0,03	0	0	1	0,03
	Capra sp.	41	1,33	3	1,2	44	1,32
Megaloceros giganteus	giant deer	23	0,75	0	0	23	0,69
Cervus elaphus	red deer	126	4,09	3	1,2	129	3,87
Dama dama	fallow deer	2	0,06	0	0	2	0,06
Rangifer tarandus	reindeer	0	0	1	0,4	1	0,03
Capreolus capreolus	roe deer	3	0,1	1	0,4	4	0,12
	Cervid sp.	144	4,67	8	3,2	152	4,56
Sus scrofa	wild boar	2	0,06	0	0	2	0,06
Indeterminate remains							
	carnivore large	51	1,65	15	6	66	1,98
	carnivore medium	53	1,72	1	0,4	54	1,62
	carnivore small	19	0,62	0	0	19	0,57
	ungulate large	246	7,98	14	5,6	260	7,8
	ungulate medium large	303	9,82	3	1,2	306	9,18
	ungulate small medium	52	1,69	2	0,8	54	1,62
	ungulate small	8	0,26	0	0	8	0,24
	mammal unknown	1341	43,48	39	15,6	1380	41,4
Total		**3084**		**250**		**3334**	

Supplementary Table 11: Number of specimens (NSP) and percentage for different weathering stages from Layers I and J.

Weathering stage	Layer I		Layer J	
	NSP	**%**	**NSP**	**%**
0	1827	60.7	181	79.4
1	967	32.1	39	17.1
2	201	6.7	7	3.1
3	10	0.3	1	0.4
4	4	0.1	0	0

Supplementary Table 12: Number of specimens (NSP) and percentage of bone surface remaining for Layers I and J.

Bone surface readability	Layer I		Layer J	
	NSP	**%**	**NSP**	**%**
0%	6	0.2	0	0.0
<50%	414	14.5	13	14.4
>50%	1629	57.1	40	44.4
100%	805	28.2	37	41.1

Supplementary Table 13: Number of specimens with carnivore modifications in Layers I and J.

Taxon	Layer I			Layer J		
	Tooth scratch	**Tooth pit**	**Scalloping**	**Tooth scratch**	**Tooth pit**	**Scalloping**
Leporid sp.		1				
Canis lupus			1			
Crocuta spelaea	1	1		1	1	
Ursus spelaeus		3	5		1	1
Ursus sp.		1	1			
carnivore large		1				
carnivore small		1	1			
Equus ferus		1				
Bos primigenius	1	1	1			
Bos Bison sp.		1	1			
Rupicapra rupicapra		1	1			
Cervus elaphus		2	1			
Capreolus capreolus		1				
Cervid sp.		2				
ungulate large	1	2	1		1	
ungulate medium large	1	3	1			
ungulate small medium	1		1			
mammal unknown	5	9	1	1		
Total	10	31	16	2	3	1

Supplementary Table 14: Number of specimens with anthropogenic modifications from Layers I and J.

Taxon	Layer I					Layer J				
	cut	anvil	percussion	scraping	retoucher	cut	anvil	percussion	scraping	retoucher
bird unknown	1									
Leporid sp.	2									
Canis lupus	2			1						
Vulpes vulpes	1			1						
Panthera leo spelaea	1									
Crocuta crocuta spelaea	1	1				1				
Ursus spelaeus	2	2	3	3	4					
Ursus arctos	1									
Ursus sp.	12		1	3	4					
carnivore large	5	1	1	2						
carnivore medium	1			2						
carnivore small	2									
Equus ferus	1				1					
Equid sp.	5	2	2	3	1					
Bos primigenius	16	7	7	1	4				1	
Bison priscus	1									
Bos Bison sp.	36	11	8	12	7	1	1	2	2	1
Capra ibex	4									
Rupicapra rupicapra	1			1						
Capra caucasica	1									
Capra sp.	8	1	1							
Megaloceros giganteus	2	1	1	5	5					
Cervus elaphus	3	4	5	8	2					
Capreolus capreolus	1									
Cervid sp.	26	1	3	6	1	1				
ungulate large	31	8	12	8	3					
ungulate medium large	44	8	1	9	4				1	
ungulate small medium	8					1				
ungulate small	1									
mammal unknown	88	17	19	7	3	2	1	2		
Total	**308**	**64**	**64**	**72**	**39**	**6**	**2**	**4**	**4**	**1**

Supplementary Table 15: Worked and/or anthropogenically modified osseous pieces from Layers I and J at Bacho Kiro Cave.

Unit ID	Layer	Type	Taxon	Location Fig. 4
AA7-1194	N1-I	pendant	*Ursus spelaeus*	*3*
BB7-1074	N1-I	pendant	*Ursus spelaeus*	*8*
BB7-300	N1-I	pendant	*Ursus spelaeus*	*4*
CC7-2858	N1-I	pendant	*Ursus spelaeus*	*7*
CC7-314	N1-I	pendant	*Ursus spelaeus*	*5*
BB8-1748	N1-I	pendant	*Ursus spelaeus*	*2*
CC8-1571	N1-I/J	pendant	*Ursus spelaeus*	*6*
CC8-770	N1-I	pendant	*Ursus spelaeus*	*10*
BB7-1041	N1-I	pendant	*Ursus spelaeus*	
BB8-2302	N1-I	pendant	*Ursus spelaeus*	*9*
F5-95	I	pendant	*Ursid sp.*	
AA8-2167	N1-J	pendant	ungulate	*1*
AA8-222	N1-H/I	bead	Elephantidae **	*17*
BB7-820	N1-I	awl	*Cervid/Saiga/Roe deer**	*11*
CC8-1091	N1-I	awl	Indeterminate*	*12*
CC7-381	N1-I	awl	Indeterminate*	*15*
AA8-1434	N1-I	*lissoir* ("smoother")	Indeterminate*	*14*
CC7-180	N1-I	spatulate	Indeterminate*	*13*
F6-622	J	*lissoir* ("smoother")	*Bos/Bison**	*16*
F5-182	I/J	incised	*Bos/Bison**	
CC7-2542	N1-J	incised	*Bos/Bison*	
BB8-193	N1-I	incised and pointed tool	*Ursidae**	
AA7-158	N1-I	intermediate tool	*Bos/Bison**	
AA7-31	N1-H/I	intermediate tool	Indeterminate*	

* identified using ZooMS.
** morphological and/or proteomic identification.

Supplementary Discussion 7: Radiocarbon dating

Supplementary table 16: Pretreatment information and accelerator mass spectrometer (AMS) radiocarbon dates of hominins included in Fig 2 (main text). Dates have been rounded to nearest 10 years and calibrated in OxCal v4.3[56] using the IntCal13 dataset[55]. Under Pretreatment: 'Longin' denotes samples pretreated with modified versions of the Longin collagen extraction method[47]; 'UF' indicates gelatinised collagen extracts were ultrafiltered[47-49] to remove small molecular weight contaminants; 'HYP' indicates individual hydroxyproline amino acids were separated from gelatinised collagen for compound-specific dating[130].

Sample	AMS lab number	Pretreatment	Collagen yield	C:N	¹⁴C age (BP)	1σ calibrated range (cal BP)	2σ calibrated range (cal BP)	References
Châtelperronian Neanderthals								
Grotte du Renne AR-14	MAMS-25149	Longin + UF	3.9%	3.2	36840 ± 660	41980-49840	42430-40180	5
Saint-Césaire SP 28	OxA-18099	Longin + UF	0.8%	3.3	36200 ± 750	41550-40110	42150-39340	6
Early Upper Palaeolithic *Homo sapiens*								
Bacho Kiro Cave CC7-335	ETH-86772	Longin + UF	11.9%	3.1	42450 ± 510	46190-45250	46790-44830	3
Bacho Kiro Cave CC7-2289	ETH-86771	Longin + UF	4.2%	3.1	40600 ± 420	44580-43720	44980-43340	3
Bacho Kiro Cave BB7-240	ETH-86770	Longin + UF	9%	3.1	41850 ± 480	45660-44800	46130-44400	3
Bacho Kiro Cave AA7-738	ETH-86769	Longin + UF	12.3%	3.1	39750 ± 380	43760-43050	44210-42810	3
Pestera cu Oase 1	GrA-22810	Longin	4%	2.6	34290 ± 970	40040-37610	41070-36470	131
Kostenki 14	OxA-X-2395-15	HYP	-	5.1*	33250 ± 500	38220-36810	38690-36260	130
Kostenki 1	OxA-15055	Longin + UF	9.6%	3.2	32070 ± 190	36200-35760	36380-35520	132
Bacho Kiro Cave F6-597	ETH-86773+ AIX-12025	Longin + UF	4.2%	3.2	31660 ± 140	35750-35340	35970-35140	3
Bacho Kiro Cave BK 1653	ETH-86768+ AIX-12024	Longin + UF	11.8%	3.2	30570 ± 120	34690-34380	34820-34210	3
Ust'-Ishim	OxA-25516+ OxA-30190	Longin + UF	7.7% 10%	3.2 3.3	41400 ± 950	45750-44010	46840-43210	28
Tianyuan Cave	BA-03222	-	-	-	34430 ± 510	39560-38450	40260-37760	133

+ Multiple dates from the same bone/collagen extract were combined using the R_combine feature in OxCal[56].

*Whereas well-preserved collagen extracts are expected to have C:N ratios In the range of 2.9-3.6[134], the theoretical C:N ratio of HYP is 5.0[130].

References

94   Ginter, B. & Kozlowski, J. K. in *Excavation in the Bacho Kiro Cave (Bulgaria): Final Report* (ed. Kozłowski, J. K.) 169-172 (Państwowe Wydawnictwo Naukowe, 1982).

95   Kozlowski, J. K. & Otte, M. The formation of the Aurignacian in Europe. *Journal of Anthropological research* **56**, 513-534 (2000).

96   Zilhão, J. & d'Errico, F. The chronology and taphonomy of the earliest Aurignacian and its implications for the understanding of Neanderthal extinction. *Journal of World Prehistory* **13**, 1-68 (1999).

97   Teyssandier, N. *Les débuts de l'Aurignacien en Europe: discussion à partir des sites de Geissenklösterle, Willendorf II, Krems-Hundssteig et Bacho Kiro*. (University of Paris X-Nanterre, 2003).

98   Rigaud, J.P. & Lucas, G. The first Aurignacian technocomplexes in Europe: a revision of the Bachokirian. *Towards a definition of the Aurignacian. Trabalhos de Arqueologia* **45**, 277-284 (2006).

99   Volkman, P. in *Prehistory and paleoenvironments in the central Negev, Israel* Vol. 3 (ed. Marks, A. E.) 127-190 (Department of Anthropology, Southern Methodist University, 1983).

100   Teyssandier, N. Questioning the first Aurignacian: Mono or multicultural phenomenon during the formation of the Upper Paleolithic in Central Europe and the Balkans. *Anthropologie* **XLIV**, 9-29 (2006).

101   Kozlowski, J. K. in *Rethinking the Human Revolution: new behavioural and biological perspectives on the origin and dispersal of modern humans* (eds. Mellars, P., Boyle, K., Bar-Yosef, O., & Stringer, C.) 317-328 (McDonald Institute for Archaeological Research, 2007).

102   Tsanova, T. *Les débuts du Paléolithique supérieur dans l'Est des Balkans. Réflexion à partir de l'étude taphonomique et techno-économique des ensembles lithiques des sites de Bacho Kiro (couche 11), Temnata (couches VI et 4) et Kozarnika (niveau VII)*. (Archaeopress, 2008).

103   Kuhn, S. L., Stiner, M. C. & Güleç, E. Initial Upper Palaeolithic in south-central Turkey and its regional context: a preliminary report. *Antiquity* **73**, 505-517 (1999).

104   Bailey, S. E., Benazzi, S., Buti, L. & Hublin, J. J. Allometry, merism, and tooth shape of the lower second deciduous molar and first permanent molar. *American Journal of Physical Anthropology* **159**, 93-105 (2016).

105   Bailey, S., Skinner, M. M. & Hublin, J. J. What lies beneath? An evaluation of lower molar trigonid crest patterns based on both dentine and enamel expression. *American Journal of Physical Anthropology* **145**, 505-518 (2011).

106   Molnar, S. Human tooth wear, tooth function and cultural variability. *American Journal of Physical Anthropology* **34**, 27-42 (1971).

107   Turner, C., Nichol, C. & Scott, G. in *Advances in Dental Anthropology* (eds. Kelley, M. & Larsen, C.) 13-31 (Wiley Liss, 1991).

108   Briggs, A. W. *et al.* Patterns of damage in genomic DNA sequences from a Neandertal. *Proceedings of the National Academy of Sciences USA* **104**, 14616-14621 (2007).

109   Sawyer, S., Krause, J., Guschanski, K., Savolainen, V. & Pääbo, S. Temporal Patterns of Nucleotide Misincorporations and DNA Fragmentation in Ancient DNA. *PLoS ONE* **7**, e34131 (2012).

110   Posth, C. *et al.* Pleistocene Mitochondrial Genomes Suggest a Single Major Dispersal of Non-Africans and a Late Glacial Population Turnover in Europe. *Current Biology* **26**, 827-833 (2016).

111   Smith, G. M. Taphonomic resolution and hominin subsistence behaviour in the Lower Palaeolithic: differing data scales and interpretive frameworks at Boxgrove and Swanscombe (UK). *Journal of Archaeological Science* **40**, 3754-3767 (2013).

112   Smith, G. M. Neanderthal megafaunal exploitation in Western Europe and its dietary implications: A contextual reassessment of La Cotte de St Brelade (Jersey). *Journal of Human Evolution* **78**, 181-201 (2015).

113   Smith, G. M. Middle Palaeolithic subsistence: the role of hominins at Lynford, Norfolk, UK. *Quaterly International* **252**, 68-81 (2012).

114   Fisher, J. W. Bone surface modifications in zooarchaeology. *Journal of Archaeological Method and Theory* **2**, 7-68 (1995).

115   Fernandez-Jalvo, Y. & Andrews, P. *Atlas of Taphonomic Identifications: 1001+ Images of Fossil and Recent Mammal Bone Modification*. (Springer, Dordrecht, 2016).

116   Binford, L. R. *Bones: Ancient Men and Modern Myths*. (Academic Press, 1981).

117   Blumenschine, R. J., Marean, C. W. & Capaldo, S. D. Blind Tests of Inter-analyst Correspondence and Accuracy in the Identification of Cut Marks, Percussion Marks, and Carnivore Tooth Marks on Bone Surfaces. *Journal of Archaeological Science* **23**, 493-507 (1996).

118   d'Errico, F., Giacobini, G. & Puech, P. Varnish replicas: a new method for the study of worked bone surfaces. *International Journal of Skeletal Research* **9-10**, 29-51 (1984).

119   Olsen, S. L. Analytical Approaches to the Manufacture and Use of Bone Artifacts in Prehistory. (University of London, 1984).

120   Sidéra, I. *Les Assemblages Osseux en Bassins Parisien et Rhénan du VIe au IVe Millénaire B.C. Histoire, Techno-économie et Culture*. (Université de Paris I., 1993).

121   Christidou, R. *Outils en os Neolithiques du Nord de la Grece: Etude Technologique*. (Universite Paris X, 1999).

122   Kahlke, R. D. *The History of the Origin, Evolution and Dispersal of the Late Pleistocene Mammuthus-Coelodonta Faunal Complex in Eurasia (Large Mammals)*. (Mammoth Site of Hot Springs, 1999).

123   Popov, V. in *The Pleistocene: Geography, Geology, and Fauna* (ed. Gareau, J. & Huard, G.) (Nova Science Publishers Inc, 2018).

124   Spassov, N. & Popov, V. in History of the Formation of the Bulgarian Mammal Fauna. (eds. *Miteva, S., Mihova, B., Georgiev, K., Petrov, B. , Vansink, D.)* 31-46 (Arnhem, 2007).

125   Stiner, M. C., Kuhn, S. L., Weiner, S. & Bar-Yosef, O. Differential Burning, Recrystallization, and Fragmentation of Archaeological Bone. *Journal of Archaeological Science* **22**, 223-237 (1995).

126   Riel-Salvatore, J. in *Sourcebook of Paleolithic Transitions* (eds. Camps, M. & Chauhan, P.) 377-396 (Springer, 2009).

127   d'Errico, F., Zilhao, J., Baffier, D., Julien, M. & Pelegrin, J. Neandertal acculturation in Western Europe? A critical review of the evidence and its interpretation. *Current Anthropology* **39**, S1-S44 (1998).

128   Derevianko, A. P. & Rybin, E. P. The earliest representations of symbolic behaviour by Paleolithic humans in the Altai Mountains. *Archaeology, Ethnology and Anthropology of Eurasia* **4**, 27-50 (2003).

129   Guadelli, A. *Kostni artefakti ot paleolita v Bulgaria (Les artefacts en matière dure animale du paléolithique Bulgare)*. (NAIM, 2011).

130   Marom, A., McCullagh, J. S. O., Higham, T. F. G., Sinitsyn, A. A. & Hedges, R. E. M. Single amino acid radiocarbon dating of Upper Paleolithic modern humans. *Proceedings of the National Academy of Sciences* **109**, 6878-6881 (2012).

131   Trinkaus, E. *et al.* An early modern human from the Peştera cu Oase, Romania. *Proceedings of the National Academy of Sciences of the United States of America* **100**, 11231-11236 (2003).

132   Higham, T. F. G., Jacobi, R. M. & Ramsey, C. B. AMS Radiocarbon dating of ancient bone using ultrafiltration. *Radiocarbon* **48**, 179-195 (2006).

133   Shang, H., Tong, H. W., Zhang, S. Q., Chen, F. Y. & Trinkaus, E. An early modern human from Tianyuan cave, Zhoukoudian, China. *Proceedings of the National Academy of Sciences of the United States of America* **104**, 6573-6578 (2007).

134   van Klinken, G. J. Bone collagen quality indicators for palaeodietary and radiocarbon measurements. *Journal of Archaeological Science* **26**, 687–695 (1999).